

29. A. Dobry, J. A. Riera, *Phys. Rev. B* **56**, R2912 (1997).
30. S. Miyahara, K. Ueda, *J. Phys. Soc. Jpn.* **69** (suppl. B), 72 (2000).
31. M. Takigawa, N. Motoyama, H. Eisaki, S. Uchida, *Phys. Rev. B* **55**, 14129 (1997).
32. F. Tedoldi, R. Santachiara, M. Horvatić, *Phys. Rev. Lett.* **83**, 412 (1999).
33. M.-H. Julien et al., *Phys. Rev. Lett.* **84**, 3422 (2000).
34. We thank J. L. Gavilano and P. Van der Linden for help

with the very low temperature measurements, K. Ueda and M. Imada for useful discussions, and M.-H. Julien and Y. Tokunaga for technical assistance. M.T. and K.K. thank Grenoble High Magnetic Field Laboratory for their hospitality during the course of these experiments. Supported in part by Grants-in-Aid for Scientific Research from the Japan Society for the Promotion of Science; the Ministry of Education, Science and Culture, Japan; and the Swiss National Fund.

Supporting Online Material

www.sciencemag.org/cgi/content/full/298/5592/395/DC1
SOM Text
Fig. S1
Tables S1 and S2

13 June 2002; accepted 2 September 2002

Stimulated Raman Scattering in Hydrogen-Filled Hollow-Core Photonic Crystal Fiber

F. Benabid,* J. C. Knight, G. Antonopoulos, P. St. J. Russell

We report on stimulated Raman scattering in an approximately 1-meter-long hollow-core photonic crystal fiber filled with hydrogen gas under pressure. Light was guided and confined in the 15-micrometer-diameter hollow core by a two-dimensional photonic bandgap. Using a pulsed laser source (pulse duration, 6 nanoseconds; wavelength, 532 nanometers), the threshold for Stokes (longer wavelength) generation was observed at pulse energies as low as 800 ± 200 nanojoules, followed by a coherent anti-Stokes (shorter wavelength) generation threshold at 3.4 ± 0.7 microjoules. The pump-to-Stokes conversion efficiency was $30 \pm 3\%$ at a pulse energy of only 4.5 microjoules. These energies are almost two orders of magnitude lower than any other reported energy, moving gas-based nonlinear optics to previously inaccessible parameter regimes of high intensity and long interaction length.

A long-standing challenge in nonlinear optics is the maximization of nonlinear interactions between laser light and low-density media such as gases. The requirements for efficient nonlinear processes are high intensity at low power, a long interaction length, and a good-quality transverse beam profile. A conceptual structure capable of delivering all these requirements simultaneously is a perfectly guiding, hollow-core waveguide supporting a single transverse mode with low attenuation losses. Theoretically, this could be realized by using a perfect metal. However, the attenuation in real metals at optical frequencies is too high. We report here the use of a hollow-core photonic crystal fiber (HC-PCF) (1) to achieve efficient stimulated Raman scattering (SRS) in hydrogen gas.

Unlike in hollow fiber capillaries, light is trapped in an HC-PCF by a two-dimensional photonic band gap (PBG) created by a "photonic crystal" of microcapillaries filling the region around the hollow core (2). Although theory shows that light can be guided in a single transverse mode without loss, typical current HC-PCFs display attenuation losses on the order 1 dB/m. Such low attenuation, allied with a very small core area ($\sim 100 \mu\text{m}^2$), make HC-PCF a promising "host" for

Raman active gases, offering ultralong interaction lengths while keeping the laser beam tightly confined in a single mode.

A number of conventional approaches have been used to enhance SRS in gases. These include focusing a laser beam into the gas with suitable optics, using a $\sim 200\text{-}\mu\text{m}$ -bore fiber capillary to confine the gas and provide some degree of guidance for the light (3), and employing a gas-filled high-finesse Fabry-Pérot cavity to increase the interaction length (4). It is instructive to compare these with HC-PCF, using the figure of merit $f_{\text{om}} = L_{\text{int}}\lambda/A_{\text{eff}}$, where L_{int} is the effective constant-intensity interaction length and A_{eff} is the effective cross-sectional area. Focusing a la-

ser beam with conventional optics produces approximately constant high intensity over a distance equal to twice the Rayleigh length $z_R = \pi w_0^2/\lambda$, where w_0 is half the beam width at the focus and λ is the vacuum wavelength; in this case, $f_{\text{om}} \sim 16$. In a fiber capillary, the figure of merit takes the form

$$f_{\text{om}} = \frac{6.8a(n^2 - 1)}{\lambda \pi \sqrt{n^2 + 1}} \quad (1)$$

where n is the refractive index of the glass, and we used the results reported in (5). This increases in a linear fashion with bore radius a , indicating that small-core capillaries make poor waveguides. For a hollow-core PCF, the figure of merit takes the form

$$f_{\text{om}} = \frac{\lambda}{\pi a^2 \alpha} \quad (2)$$

where α is the exponential attenuation rate of the intensity. These three expressions are plotted (Fig. 1) for silica glass ($n = 1.46$) at a wavelength of 532 nm.

The HC-PCF has clear advantages, particularly when the bore is small. At a diameter of 10 μm , for example, a free-space beam is preferable to a capillary, whereas an HC-PCF with a loss of 0.3 dB/m is almost 10,000 times more effective. Improvements in all sorts of nonlinear laser-gas interactions should become possible, such as ultralow-threshold SRS in gases.

SRS is a two-photon linear inelastic light-scattering process, in which an incoming photon interacts with a coherently excited state of the system (in our case, one of the vibrations of a hydrogen molecule). As a

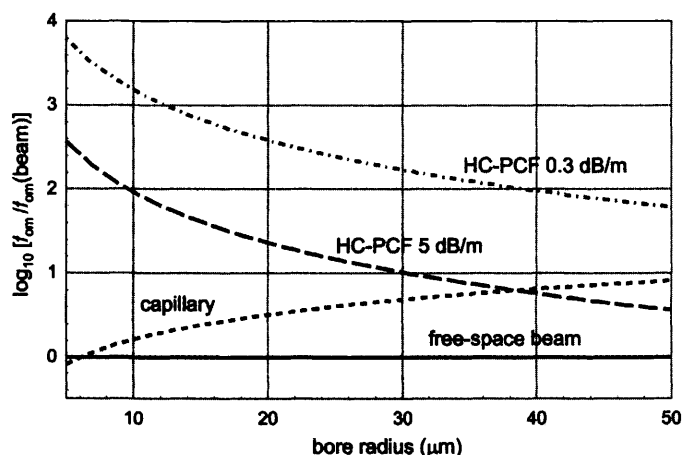


Fig. 1. Figures of merit for a hollow capillary and two HC-PCFs, relative to the value for a free-space beam. At a bore radius of 5 μm , the HC-PCF is almost 10,000 times better.

Optoelectronics Group, Department of Physics, University of Bath, Claverton Down, Bath BA2 7AY, UK.

*To whom correspondence should be addressed. E-mail: pysab@bath.ac.uk

REPORTS

result of this interaction, a frequency down-converted (Stokes) or an upconverted (anti-Stokes) photon is emitted. SRS is useful for laser frequency conversion, high-resolution spectroscopy, pulse compression (6, 7), and phase conjugation (8). To achieve reasonable conversion efficiency, however, high-power lasers (≥ 1 MW) are required, severely limiting the potential applications of SRS in nonlinear optics and technology. The threshold power for gas-SRS can be reduced by using multipass cells such as a high-finesse Fabry-Pérot resonator (4), in which first-order Stokes (longer wavelength) emission was reported at a continuous wave input pump power

of only 400 μ W. This was achieved in an ~ 8 -cm-long doubly resonant hydrogen-filled resonator, with an intracavity intensity enhancement of 25×10^3 . Limitations of this approach are the large effective beam area A_{eff} (~ 0.4 mm 2) and the need to keep the (very sharp) cavity resonance tightly locked to the pump laser frequency. Moreover, the doubly resonant design of the Fabry-Pérot resonator means that efficient frequency conversion is limited to a single Stokes signal only. The only viable conventional alternative, as outlined above, is to use a gas-filled hollow fiber capillary; this is at best a compromise because, for low leakage of light, the

mode area must be large ($\sim 30,000$ μ m 2). Such large-bore capillaries also support multiple leaky modes, causing problems of transverse mode instability.

Our HC-PCF had a core diameter of 15 μ m, and was filled with hydrogen gas and pumped with a Q-switched single-mode frequency-doubled Nd:YAG (neodymium/yttrium aluminum garnet) laser operating at a wavelength of 532 nm, with a repetition rate of 20 Hz and a pulse duration of 6 ns. After passing through a neutral density filter and a telescope to optimize the coupling efficiency, the laser beam was divided in two at a 50/50 beamsplitter (Fig. 2). One beam was sent to a power meter, and the second beam was coupled to the lowest-order air-guided mode of the HC-PCF (9) using a $\times 4$ objective lens.

The Raman amplifier consisted of two identical gas cells (GCs). An anti-reflection-coated window was sealed to one face of each cell, and one fiber was end-mounted on the facing window. The input cell (GC 1) was charged with hydrogen at a given pressure, and the output cell (GC 2) gradually filled, through the differential pressure gradient, until equilibrium was reached. We achieved pressures as high as 50 bar (the limit of our pressure regulator) without damage. The results presented here were all taken at a pressure of 17 bar (1 bar = 10,000 Pa). The light emerging from the fiber was split into two beams. One was sent either to an optical spectrum analyzer or to a fast photodetector to monitor the total transmitted power. The other was sent to a set of calibrated fast photodetectors in front of which was placed an appropriate 10-nm bandpass color filter (CF) to separate out the pump, Stokes, and anti-Stokes signals. This setup allowed rapid characterization of the generated Stokes and anti-Stokes signals as functions of pump power, interaction length, and gas pressure.

The fiber itself was fabricated with the capillary stacking technique (10), its core being formed from seven missing capillaries. The cladding structure was somewhat different from the triangular and honeycomb HC-PCF structures so far reported (11, 12) and consisted of fine silica webs arranged in a Kagomé lattice surrounded by air (Fig. 3B). The thickness of the silica webs was ~ 500 nm. The fiber had an outer diameter of 170 μ m, a core diameter of ~ 15 μ m, and a lattice constant of 5 μ m. The air-filling factor was measured to be $\sim 83\%$.

Compared to the HC-PCF we previously reported (1), this structure has a much wider transmission bandwidth, covering the whole visible/infrared range. Figure 3A shows the loss over the 400- to 1700-nm range, measured with a white light source. The minimum value is ~ 1 dB/m and occurs at 1307 nm. Excluding the loss peak at around 1390 nm (due to the presence of OH in the glass

Fig. 2. Experimental setup. BS, beamsplitter; OBJ, objective; GC, gas cell; CF, bandpass color filter; PD, fast photodetector; OSA, optical spectrum analyzer.

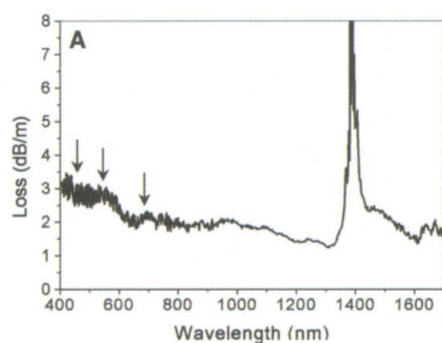
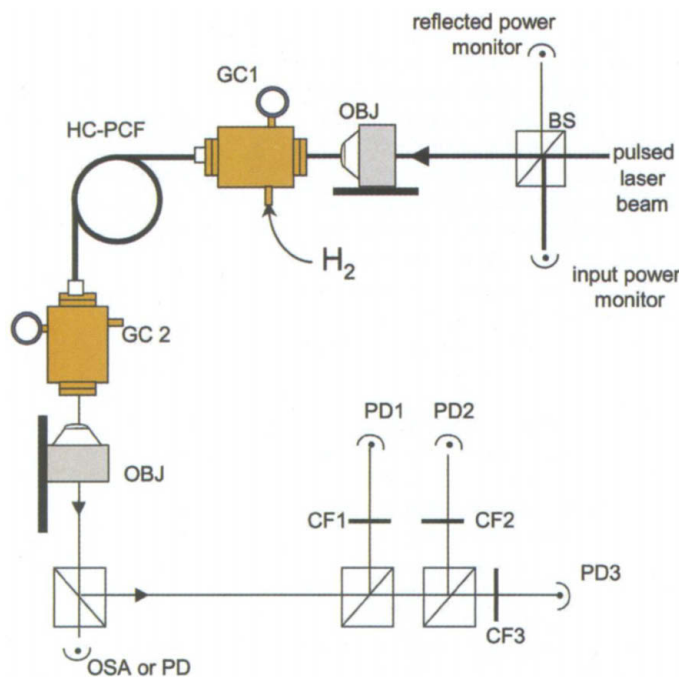
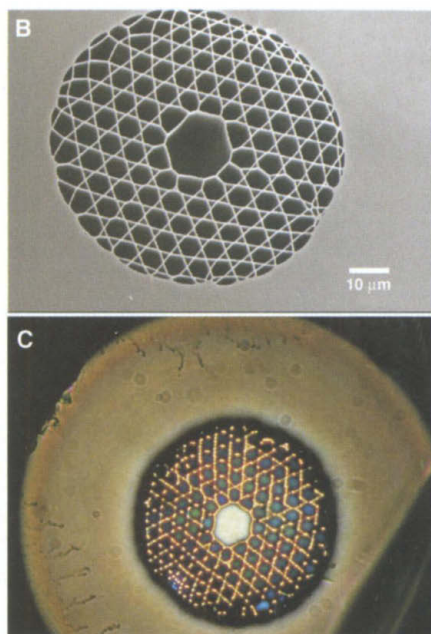


Fig. 3. (A) The measured loss of the HC-PCF. The large peak at ~ 1390 nm is attributed to OH absorption. The arrows point to the loss at the wavelengths of the pump (532 nm), the Stokes (683 nm), and the anti-Stokes (435 nm). (B) Scanning electron micrograph of an HC-PCF with an outer diameter of 170 μ m. (C) The exit end of a ~ 6 -cm-long HC-PCF illuminated by white light, as seen under an optical microscope.



and water in the holes), the fiber loss is less than 3 dB/m over our whole detectable spectral range (350 to 1700 nm). This is corroborated by the bright white-colored guided mode in the core (optical micrograph in Fig. 3C).

The measurements were carried out for different fiber lengths by repeated cut-back of a 920-mm-long fiber. For each length, the transmitted total power, pump, Stokes, and anti-Stokes powers were measured for different input powers. At every point, the spectra of the transmitted and reflected beams were also measured.

In the evolution of the transmitted spectrum as a function of input power (Fig. 4A), the growth of the first-order Stokes (683 nm), followed by an anti-Stokes signal (~ 435 nm) due to parametric four-wave mixing, can be seen. No backward SRS was observed (13, 14), nor were any rotational Raman signals seen. This is not surprising, because we used a linearly polarized laser beam, and in the steady-state regime, the rotational Raman components are known to be most efficiently excited at pressures lower than 17 bar (0 to 10 bar). The near-field intensity patterns of the three spectral components were measured at different fiber lengths (Fig. 4E). For all three wavelengths, the mode profile peaks in the center of the core, indicating a fundamental guided mode.

An unusual feature of the data is that the total transmitted energy (Fig. 4B), plotted against coupled energy E_c , saturates in the range $3 \mu\text{J} < E_c < 4 \mu\text{J}$, with the exact value depending on the fiber length, indicating the existence of a strong nonlinear loss mechanism. The transmission is recovered when the power is reduced, so this phenomenon is not caused by damage to the fiber. Nor is it caused by conversion to higher-order Stokes or anti-Stokes bands, for neither the second-order Stokes (~ 953.6 nm) nor the second-order anti-Stokes (368.9 nm) was observed, despite the fact that their wavelengths lay within the transmission band of the HC-PCF. A clue to its origin lies in the observation that, for $E_c > 4 \mu\text{J}$, bright scattering of both the pump and the Stokes light was visible through the side of the fiber, persisting for ~ 10 cm beyond its starting point, which moved closer to the input end as E_c increased.

We attribute the nonlinear loss to Raman-enhanced self-focusing, which can occur at low peak powers (~ 650 W in our experiments). It has been pointed out that self-focusing in gas-filled capillaries can cause transfer of energy from the fundamental mode to the next higher-order mode (15). Although the HC-PCF is close to single mode, it does support a next-higher order mode with a measured attenuation of 57 dB/m. Any light converted to this mode from the fundamental mode will be very

rapidly lost, leading to strong attenuation of the transmitted Stokes and pump light. An intriguing feature of the data is that the anti-Stokes signal does not display the same attenuation.

The transmitted energies in the pump (532 nm), Stokes (683 nm), and anti-Stokes (~ 435 nm) signals are plotted against E_c for $z = 17$ cm (Fig. 4C). The input energies for Stokes transmission, measured for different fiber lengths, were $E_c = 800 \pm 200$ nJ (~ 133 W peak power or $16 \mu\text{W}$ average power). Beyond this point, the Stokes energy continues to increase, until at $E_c = 3.4 \pm 0.7 \mu\text{J}$, a weak anti-Stokes signal appears—its growth coinciding with the region where the Stokes and pump energies are comparable. This we attribute to Raman-assisted four-wave mixing.

Figure 4D shows the evolution with distance of the three signals at $E_c = 5.6 \mu\text{J}$ (~ 933 W peak power). At $z = 17$ cm (the shortest length at which we measured the signals), all three signals were apparent, indicating that conversion to the Stokes and

parametric coupling had already started (Fig. 4C). In the range of $25 \text{ cm} < z < 30$ cm, the Stokes energy builds up exponentially at almost the same rate as the drop in pump energy, as one would expect for a conventional Raman process. This is, however, accompanied by a strong increase in the anti-Stokes signal, an observation which is less easy to explain.

Understanding these phenomena requires a more detailed study, which is beyond the scope of this paper. Our current understanding is that they are the result of the interplay of SRS, Raman-enhanced four-wave mixing, and self-focusing. A simple four-wave mixing analysis of the case when the pump and Stokes powers (P_P and P_S) are strong and constant and the anti-Stokes power P_A is weak yields the result

$$P_A(z) = \left[\frac{3n_2\omega_A P_P \sqrt{P_S}}{2c n_{\text{eff}}} \right]^2 z^2 \text{sinc}^2 \frac{\partial z}{2} W \quad (3)$$

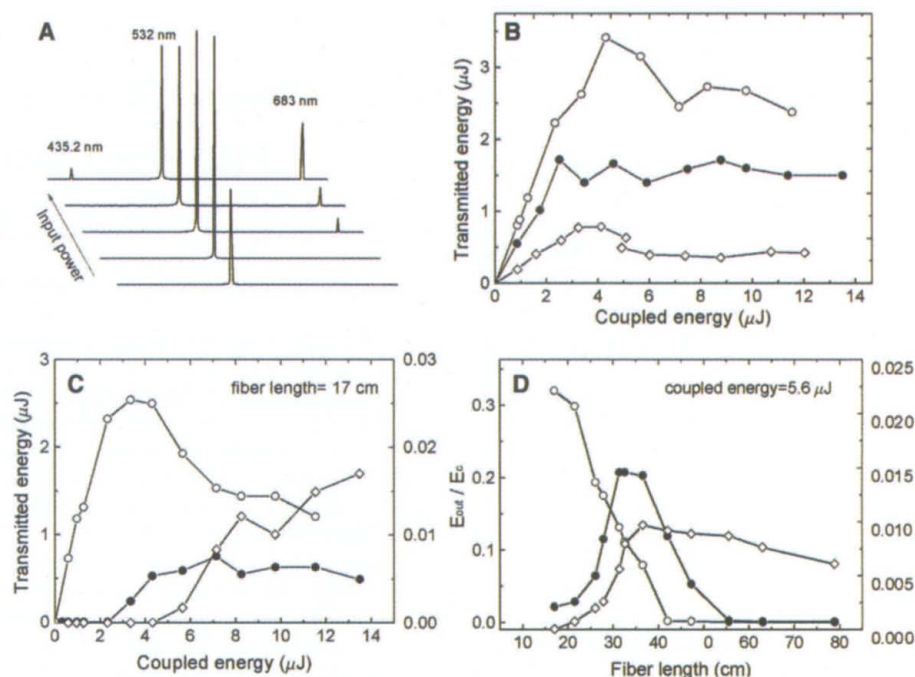


Fig. 4. (A) Evolution of the transmitted spectrum with increasing input power. The pump wavelength is 532 nm, the first-order Stokes is ~ 683 nm, and the first-order anti-Stokes is 435.2 nm. (B) Total transmitted energy is plotted versus coupled input energy for a fiber length of 17 cm (open circles), 32 cm (solid circles), and 62 cm (open diamonds), respectively. (C) Transmitted energy through a 17-cm-long HC-PCF as a function of the coupled energy for the pump (open circles) and the Stokes (solid circles) (lefthand vertical axis) and the anti-Stokes (open diamonds) (righthand vertical axis). (D) The evolution of the pump (open circles), the Stokes (solid circles), and the anti-Stokes (open diamonds) with the fiber length for a coupled energy of $5.6 \mu\text{J}$. (E) Near-field images of the transmitted pump signal (left), the Stokes signal (center), and the anti-Stokes signal (right), as recorded by a color charge-coupled device camera. The grid pattern is due to an artifact of the camera.

The phase mismatch ϑ , including nonlinear terms, is

$$\vartheta = (2\beta_p - \beta_A - \beta_s) - (3P_A + 6P_p + 6P_s) \frac{n_2 \omega_A}{2cnA_{\text{eff}}} \text{ m}^{-1} \quad (4)$$

where ω_A is the angular frequency of the anti-Stokes light, n is the refractive index, c is the velocity of light in vacuum, n_2 is the nonlinear refractive index of hydrogen, and the linear wavevectors are $\beta_i = \omega_i n_i / c$ (including the dispersion of the gas and the waveguide). For our experimental parameters ($P_p \sim P_s \sim 100$ W, $n = 1$, resonant $n_2 = 1.2 \times 10^{-17}$ m²/W, an interaction length $L \sim 0.1$ m, and $A_{\text{eff}} = 150$ μm^2), we obtain $P_A = 3 \times 10^4 \sin^2(\vartheta L) W$. Evaluation of the phase mismatch assuming (as a rough approximation) perfect metallic boundary conditions at the core boundary (12) yields $\vartheta L \sim 1000$ (the nonlinear term is negligible), which when taking the peaks of the \sin^2 function yields $P_A \sim 0.04$ W, which is some 25 times smaller than the experimental measurement of 1 W.

Equation 3 also shows that even under exact phase matching, the anti-Stokes power will increase only as the square of distance. In the data, however, the rate of growth is much faster. Indeed, the ratio $P_A / (z P_p \sqrt{P_s})^2$, which might be expected to be constant for perfect phase matching ($\vartheta = 0$), actually increases exponentially with distance in the experiments. This could be explained through a self-focusing phenomenon that reduces the effective area so as to enhance the four-wave mixing process and the phase matching. What is clear is that we are operating in a new parameter regime of extremely high, well-controlled Stokes and pump intensities over long interaction distances.

After peaking at $z \sim 35$ cm, the Stokes signal drops strongly, as already discussed. At the same time, the anti-Stokes power drops at a rate of only ~ 2 dB/m; that is, less quickly than the intrinsic linear attenuation (3 dB/m) of the HC-PCF, suggesting that some anti-Stokes gain is still present. Finally, at $z > 55$ cm, the attenuation of all three components settles down to ~ 3 dB/m, corresponding to the linear loss of the HC-PCF.

The highest observed Stokes conversion efficiency was $30 \pm 3\%$, occurring at $z = 32$ cm and $E_c = 4.5$ μJ . The conversion efficiency is evidently limited by the strong, nonlinear, loss self-focusing mechanism. At both $z = 17$ and 56 cm, the highest efficiencies occurred at $E_c \sim 3.5$ μJ , taking the values ~ 14 and 0.8%, respectively.

The reduction in threshold power for gas-SRS should allow the use of low-power solid-state diode-pumped lasers as pumps and should extend the wavelengths of solid-state sources into new spectral regions. Further orders-of-magnitude reductions in pump source require-

ments will follow from dispersion management and improvement of fiber performance. A narrower line laser source would lead to further improvements in performance. The possibility of setting a linear gradient of the pressure along the fiber might be useful for pulse chirping (16). The ability to load HC-PCF at high pressure without damage could also be of great importance for SRS in the transient regime (that is, when the pulse duration is much shorter than the dephasing time), where the Raman gain is proportional to the pressure (17).

The availability of HC-PCF is likely also to lead to rapid new progress in all types of nonlinear optics in gases and should mark the beginning of a new era in gas-based nonlinear optics.

References and Notes

1. R. F. Cregan *et al.*, *Science* **285**, 1537 (1999).
2. T. A. Birks, P. J. Roberts, P. St. J. Russell, D. M. Atkin, T. J. Shepherd, *Electron. Lett.* **31**, 1941 (1995).
3. P. Rabinowitz *et al.*, *Appl. Opt.* **15**, 2005 (1976).
4. L. S. Meng *et al.*, *Opt. Lett.* **25**, 472 (2000).
5. M. J. Renn, R. Pastel, *J. Vac. Sci. Technol. B* **16**, 3859 (1998).
6. S. E. Harris, A. V. Sokolov, *Phys. Rev. Lett.* **81**, 2894 (1998).
7. A. V. Sokolov, D. D. Yavuz, S. E. Harris, *Opt. Lett.* **24**, 557 (1999).
8. R. W. Hellwarth, *J. Opt. Sci. Am.* **68**, 1050 (1978).
9. The mode profiles of the guided modes in HC-PCF match very well with the modes in a hollow waveguide made from a perfect metal [see, for example, J. A. West *et al.*, in *Proceedings of the 26th European Conference on Optical Communication*, (VDE Verlag, Berlin, 2000), vol. 4, pp. 41–42]. The lowest-order mode has a Bessel-like modal field profile, which is strongly confined in the air core.
10. J. C. Knight *et al.*, *Opt. Lett.* **21**, 1547 (1996).
11. K. Suzuki, M. Nakazawa, "Ultrabroad band white light generation from multimode photonic bandgap fiber with an air core," paper presented at the Conference on Lasers and Electro-Optics/Pacific Rim, Chiba, Japan, 15 to 19 July 2002.
12. J. A. West, N. Venkataramam, C. M. Smith, M. T. Gallagher, in *Proceedings of the 27th European Conference on Optical Communication*, 26 September to 4 October 2001, Amsterdam, vols. 1 to 6, pp. 582–585.
13. This is partially due to the large linewidth of our laser (3 cm^{-1}) compared with the Raman linewidth $< 0.03 \text{ cm}^{-1}$.
14. Y. R. Shen, *The Principles of Nonlinear Optics* (Wiley, New York, 1984).
15. G. Tempea, T. Brabec, *Opt. Lett.* **23**, 762 (1998).
16. A. Rundquist *et al.*, *Science* **280**, 1412 (1998).
17. S. E. Harris, A. V. Sokolov, *Phys. Rev. A* **55**, R4019 (1997).
18. We thank A. George for technical support in the design and the construction of the gas cells.

22 July 2002; accepted 28 August 2002

Rapid Vapor Deposition of Highly Conformal Silica Nanolaminates

Dennis Hausmann, Jill Becker, Shenglong Wang, Roy G. Gordon*

Highly uniform and conformal coatings can be made by the alternating exposures of a surface to vapors of two reactants, in a process commonly called atomic layer deposition (ALD). The application of ALD has, however, been limited because of slow deposition rates, with a theoretical maximum of one monolayer per cycle. We show that alternating exposure of a surface to vapors of trimethylaluminum and tris(*tert*-butoxy)silanol deposits highly conformal layers of amorphous silicon dioxide and aluminum oxide nanolaminates at rates of 12 nanometers (more than 32 monolayers) per cycle. This process allows for the uniform lining or filling of long, narrow holes. We propose that these ALD layers grow by a previously unknown catalytic mechanism that also operates during the rapid ALD of many other metal silicates. This process should allow improved production of many devices, such as trench insulation between transistors in microelectronics, planar waveguides, microelectromechanical structures, multilayer optical filters, and protective layers against diffusion, oxidation, or corrosion.

Thin films are ubiquitous in modern technology. For example, processing, storage, and communication of information rely on a wide variety of thin films of semiconductors, metals, and insulators. Many different methods are used to make these films, such as various physical techniques (e.g., sputtering, evaporation, pulsed la-

ser ablation) and chemical processes (e.g., oxidation, chemical vapor deposition, electroplating, sol-gel synthesis) (1).

Assembling thin films atom by atom allows exquisite control over their composition and structure. One such technique is atomic layer deposition (ALD; also called atomic layer epitaxy), in which a vapor reacts with a surface until a monolayer has been chemisorbed (2). The reaction then stops, so the process is called "self-limiting." A second vapor then reacts with this surface in a second self-limiting reaction, thus depositing a second layer of atoms onto the

Department of Chemistry and Chemical Biology, Harvard University, 12 Oxford Street, Cambridge, MA 02138, USA.

*To whom correspondence should be addressed. E-mail: gordon@chemistry.harvard.edu